Effectiveness Assessment of Composite Repair Systems

R.I. Dmytriienko, O.L. Paliienko, P. Yukhymets, G.I. Lvov and O. Marusenko

Abstract This chapter is dedicated to the analysis of the efficiency of a given repair system using composite material wraps intended for damaged sections with volumetric surface defects of transmission pipelines (for petroleum, liquid petroleum products or natural gas). The analysis refers to the composite repair system investigated in Chapter "Inner Pressure Testing of Full-Scale Pipe Samples" and it has used the experimental data presented in Chapter "Inner Pressure Testing of Full-Scale Pipe Samples". The tests performed were defined based on the considerations in Chapter "Development of an Experimental Programme for Industrial Approbation". The efficiency assessment has been made, in the first place, considering the change of volume and the yield pressure, then taking into account the changes observed in the samples perimeter. The effect of the composite wrap on the deformations recorded for each defect and the loading diagrams have also been investigated. Finally, the efficiency has been assessed using a numerical finite-element model.

Keywords Hydrotest · Inner pressure · Pipe · Defect · Wrap

1 Evaluation Based on Change of Volume and Yield Pressure

The measurements, carried with the help of "water jacket" in the process of hydraulic loading by inner pressure of a sample, allowed sufficiently accurate registration of its volume change. Figure 1 shows the dependencies of volume change in samples I1 and I4 at initial stages of loading. It can be seen from the figure that yield start pressure $\{P_Y\}$ (volume of sample after unloading does not
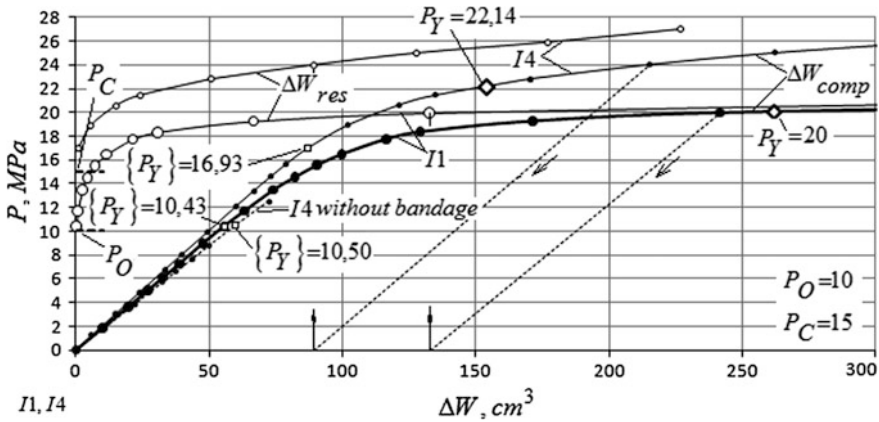
R.I. Dmytriienko (✉) · O.L. Paliienko · P. Yukhymets
E.O. Paton Electric Welding Institute, Kiev, Ukraine
e-mail: dri1@ukr.net

G.I. Lvov · O. Marusenko
National Technical University, Kharkiv Polytechnic Institute, Kharkiv, Ukraine

Fig. 1 Complete (ΔW_{comp}) and residual (ΔW_{res}) values of volume change of samples I1 and I4 at initial stages of loading in water jacket; $\{P_Y\}$ is the yield pressure, determined in water jacket; P_Y is the yield pressure, determined as a breaking point of inner pressure loading diagram; ΔW_{comp}, ΔW_{res} are the complete and residual volume changes

come back to initial state) increases 1.61 times after the wrap installation on sample I4. By this P_T pressure (determined from a hydraulic loading diagram, Fig. 6) shows a slight increase 1.1 times. It is a pressure, at which a significant part of the cylinder shell has already come to plastic deformation area. Due to the variation of pipe wall thickness and the deviation of geometry of its cross-section from circular ring, plastic deformations propagate to wider areas with pressure growth. These deformations localize in the zones of reduced cylindrical stiffness, where combination of thinning and lager curvature is observed. Diagram of hydraulic loading $P = f(T)$, as a result of reflection of the dynamic process, is not so susceptible, therefore difference between $\{P_Y\}$ and P_Y pressures can be a measure of the deviation of pipe geometry from the ideal one. Noticeable increase of $\{P_Y\} - P_Y$ difference in the case of sample I4 can indicate inclusion of the wrap in the process of plastic deformation propagation within pipe cross-section.

The increase of volume in the process of plastic deformation of cylinder sample with bottoms takes place due to reduction of the wall thickness and increase of the middle surface radius. The dependence of volume change on inner pressure, in this case, can be determined using actual deformation diagrams as

$$P = \frac{2\sigma_i s_o}{\sqrt{3} r_o e^{\sqrt{3}\varepsilon_i}}, \quad \Delta W_{comp} = \pi l_o r_o^2 \left(e^{\sqrt{3}\varepsilon_i} - 1 \right), \tag{1}$$

where s_O, r_O are the wall thickness and radius of middle surface in the initial state, l_o is the length of cylinder part, which does not change at plastic deformations, σ_i, ε_i are the stress and deformation intensity on actual deformation diagram, respectively.

The residual value of deformation intensity ε_{ires} is inserted in formula (1) when ΔW_{res} is determined.

Since Poisson's ratio $\mu = 0.5$ under plastic deformation conditions, then current values of wall thickness s and middle surface radius r can be related with initial values through logarithmic deformations ε_t or deformation intensity

$$\varepsilon_i = \frac{2}{\sqrt{3}}\varepsilon_t = \frac{2}{\sqrt{3}}\ln\frac{r}{r_O} = -\frac{2}{\sqrt{3}}\ln\frac{s}{s_O} \tag{2}$$

The results of calculations using Eqs. (1) and (2) showed close correspondence with data of sample I1 testing.

In a whole, the strengthening effect of the composite wrap in the elastic deformation area can be sufficient extent characterized by the absolute value of P_Y pressure.

Dependencies (1) and (2) can be used to determine the residual expansion coefficient (ratio of residual change of vessel volume to full one, characterizing plastic deformation level) and the current safety margin (ratio of maximum pressure, which was carried by the sample, to maximum pressure at the stage). Figure 2 gives the dependence of current safety margin and residual expansion coefficient by the example of samples I1 and I4. The inclination angle of dependence in the central part for sample I4, corresponding to stable plastic deformation (Fig. 2), is more than for sample I1. This indicates that at the same increment of pressure in this area, the sample with wrap changes in volume for a smaller value than the sample without wrap, that shows a possibility of application of indicated index for evaluation of the efficiency of installed wrap.
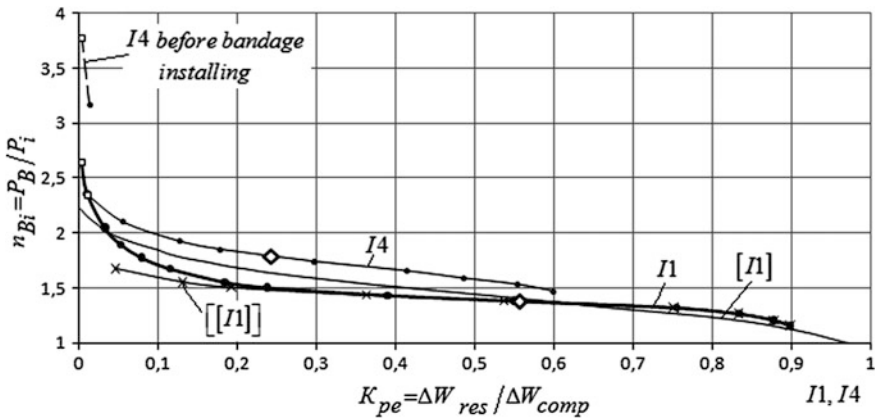
Fig. 2 Relationship of the inner pressure and safety margin on the plastic deformation level by the example of samples I1 and I4: [I1] theoretical dependence for sample I1 being calculated on actual deformation diagram; [[I1]] dependence for sample I1, if we did not take into account residual change of volume in its loading up to calibrating pressure; for other designations see Fig. 1

2 Evaluation Based on Change of Sample Perimeter

The wrap remains in elastic deformed state after fracture of sample I4 due to pipe plastic deformation. Its perimeter change along the pipe generator, out of fracture zone, is of 0.90–1.04%. It cracked at small mechanical influence, unloading took place and its perimeter was reduced. After wrap removal, residual changes of the perimeters of pipe sample I4 were 1.05–1.47%, in the case of I1 perimeter the increase was 6.8–8.6 (the maximum changes were registered in the fracture zone and the minimum ones close to the bottoms). Thus, the installation of the wraps resulted to significant (6–8 times) decrease of the circumferential residual deformations. It is necessary to note that circumferential residual deformations, obtained by measuring the distances between sample I1 punching points, were 3.3–16.4%. Considerably larger spread in deformations in comparison with the results, obtained in perimeters' measurement, is observed with variation of pipe wall thickness.

Since the value calculated for the elastic deformation is of about 0.2% at the joint work of wrap and pipe in the process of pressure release from maximum value to zero in sample I4, then carried perimeter measurements can indicate virtually complete exhaust of a deformation capability of composite material ($\sim$1.4%) at sample fracture.

3 Effect of Composite Wrap on Change of Deformations in a Defect

Figure 3 gives the results of deformation measurement in the defect and regular part of sample I3 before and after wrap installation. Loading without wrap was carried out before the occurrence of circumferential residual deformations in the defect. There are also deformation data on the wrap surface. Figure 3 also presents deformations of sample I2 for comparison.

As it can be seen, circumferential deformations in the defect area significantly decrease after some initial deformation that can be related with the removal of discontinuity flaws inside the composite and defect filling compound as well as on their mating surfaces. Installation of wraps on sample I3 does not influence the initial part of axial deformations in the defect. Axial deformations of the wrap over the defect completely match with the defect axial deformations.

Buckling resulted in a reduction of stresses in the central part of the defect, and fracture of the sample I2 took place along genetratrix with minimum thickness at the end of the defect (indicated by arrow in Fig. 4d). By this, average wall thickness in the defect zone decreased by 9%, and the wall thickness is without variations in the pipe regular part. A change of length of a measuring base in axial direction was not registered.
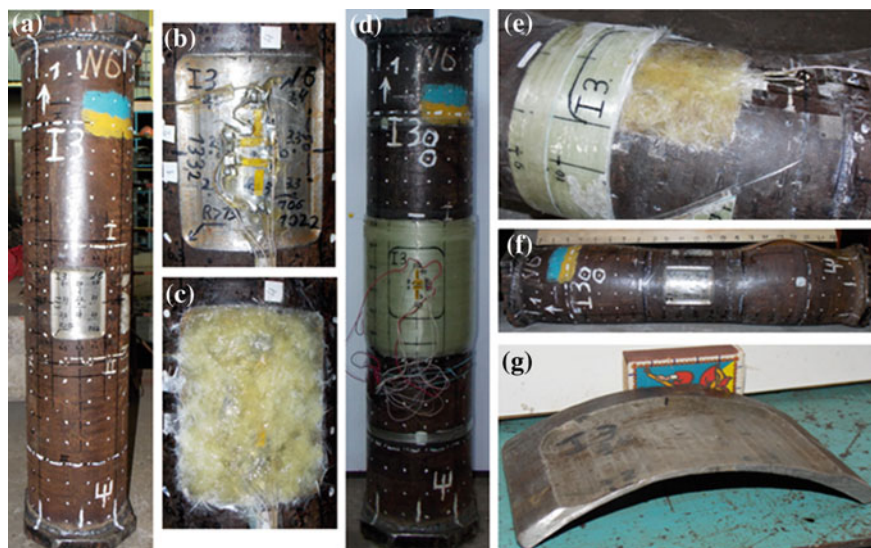
Fracture of the sample I3 took place in the uncoated section of the pipe. After wrap removal, residual circumferential deformations in the defect were 1.33% that
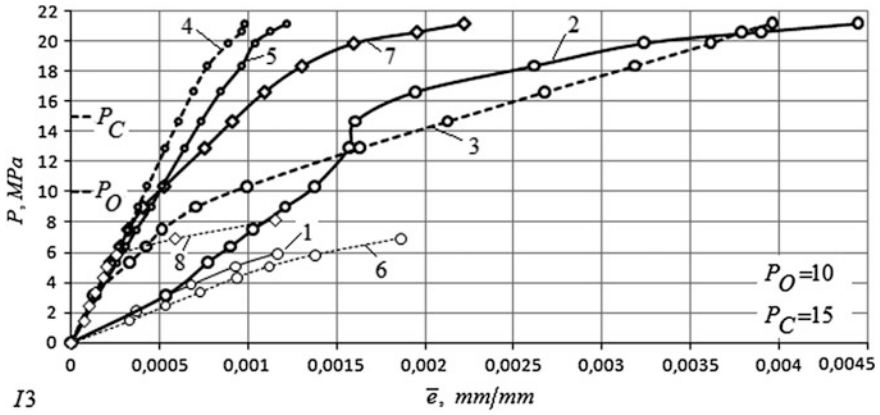
Fig. 3 Deformations of sample I3 at the initial loading stages: circumferential deformations in defect before (*1*) and after (*2*) wrap installation; at wrap in defect zone (*3*), in regular zone (*4*); for pipes in regular zone (*5*); in defect of I2 sample (*6*); axial deformations in defect after wrap installation (*7*) and in defect of sample I2 (*8*)
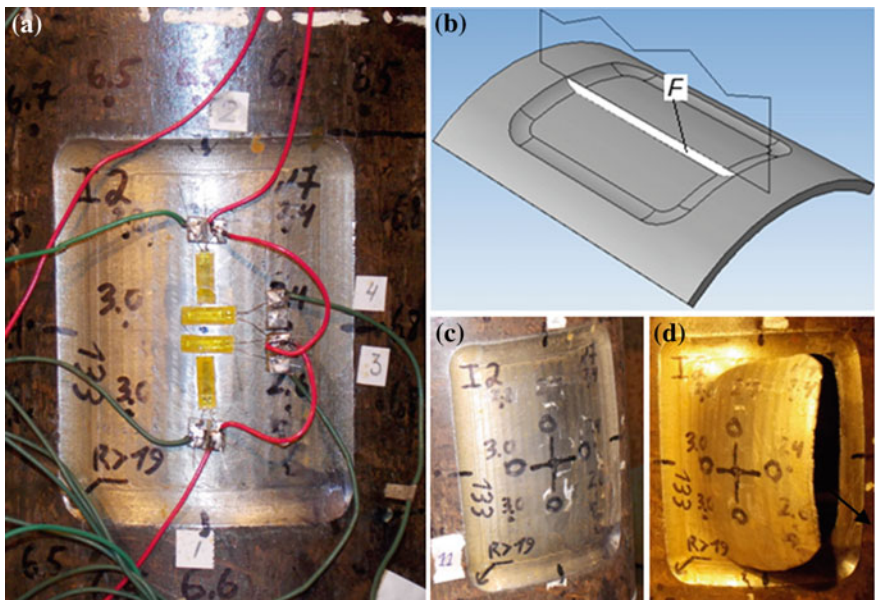
Fig. 4 Defect in sample I2: **a** with installation of resistance strain gauge; **b** area of defect in pipe axial section; **c** after penultimate stage; **d** after failure; **d** shows punching points *encircled by marker*

Fig. 5 Full-scale sample I3 before and after testing: **a** sample before installation of resistance strain gauge and wrap; **b** positioning of resistance strain gauge in defect; **c** compound-filled defects with resistance strain gauges; **d** sample before testing; **e** defect after testing; **f** sample after wrap removal, **g** cut out part of defect

verifies proportion of the selected wrap thickness and fracture pressure. Residual circumferential deformations of defect-free section of the pipe under the wrap were ≈0.2% and outside the wrap ≈11%. It is noted that residual circumferential deformations in the defect after fracture of the sample without wrap (I2) was equal to 5.36% (Fig. 5).

4   Matching of Loading Diagram

Figure 6 shows the loading diagrams before fracture of samples I1-I4, made in "pressure-time" coordinates.

Diagram of sample I1 was used as a reference. Areas of elastic and plastic deformation are well seen on the diagrams; moreover the latter corresponds to transfer in plastic state of all or main part of metal of the cylinder part of sample.

Diagram of sample I2 proves that, due to relatively small defect surface and corresponding to it plastic deformation zone, the main, non-deformed part of the pipe was subjected to elastic deformation up to fracture, which took place at a pressure two times lower than in sample I1. It should be noted that the difference of elastic parts' inclination angles in the loading diagram was not taken into account in this investigation, since it was a consequence of a series of difficult-to-consider factors, such as, for example, possible leakages in the hydraulic system.
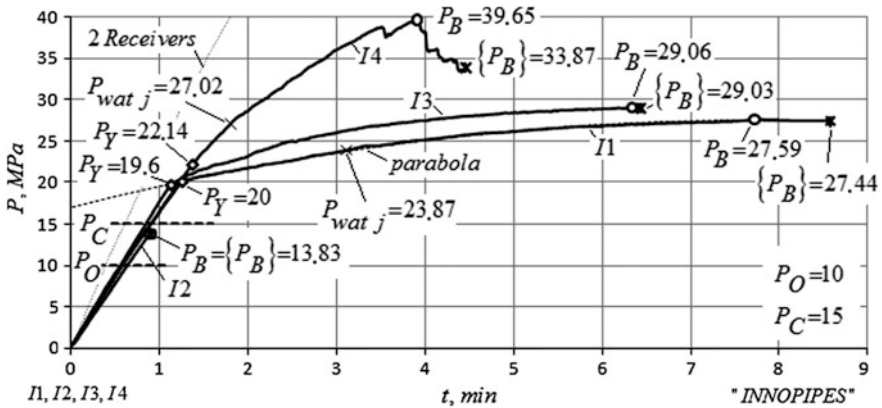
Fig. 6 Diagrams of inner pressure loading before fracture of I1, I2, I3 and I4 samples: $P_{wat.j}$ pressure to which the samples were loaded in water jacket; P_B maximum pressure; $\{P_B\}$ fracture pressure; 2 Receivers—diagram of loading of two twinned receivers without testing object; other designations see in Fig. 1

The increase of yield pressure and significant growth of fracture pressure (1.44 time) taking place simultaneously with the decrease of loading time, due to constraint of the radial movements, characterize the loading diagram of the sample simulating the strengthened part of the pipeline (I4). The rapid drop of pressure, anticipating its maximum value, obviously matches with the start of fracture of the fiberglass wraps on the boundary with a circular cutout.

The diagram of repaired sample (I3) is the closest to the reference. As it was mentioned earlier, part of the pipe under the wrap had virtually elastic deformations due to the wrap strengthening effect, except for defects. Total increase of volume, which was observed, first of all, due to plastic deformation of the non-strengthened part, significantly reduced, that, respectively, resulted to a decrease of the time of pump work before fracture. Typical points of the loading diagram, corresponding to yield and fracture pressure as well as its location (out of the wrap) clearly indicate repair efficiency.

5 Efficiency Assessment by Numerical Calculations

5.1 Selection of Finite-Element Mesh

Models of experimental pipes were built in the software package SolidWorks (Figs. 7 and 8). It is possible to execute the construction of the models close to real structures. Further models have been exporting to program complex ANSYS Workbench (WB).

Fig. 7 Solid model I2
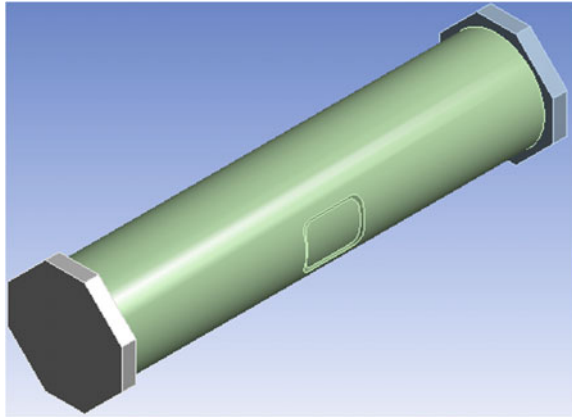
Fig. 8 Solid model I3
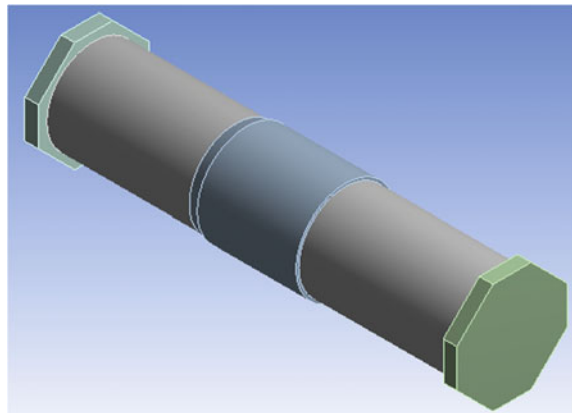
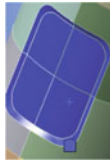**Table 1** Mechanical properties of composite material

Experiment	E (MPa)		σ_B (MPa)		ν
	Annular	Axial	Annular	Axial	
I3	48,465.21	3000	678.51	75	0.17
I4	59,850.69	3000	837.91	75	

The composite wrap was built in SolidWorks and exported to ANSYS Workbench. After that, properties of the composite were applied, and properties of anisotropy have been set. The composite material properties are present in Table 1.

The selection of finite-element mesh was conducted for I2 model. The mesh size was reduced by two times with each subsequent calculation. Mesh size was changed in the pipe plane, in the defect area and through thickness of the pipe. Example of mesh size selection is given in Table 2. Size of finite element was

Table 2 Selection of finite element mesh on the defect (axial strain)

P (MPa)	Defect, mesh size (m)			12 model defect strain		
				Axial strain		
				T1	T2	WB T1_2
5.04	0.006		0.012	0.000193	0.000211	0.000176
5.04	0.003		0.006	0.000193	0.000211	0.000182
5.04	0.0015		0.003	0.000193	0.000211	0.000202

selected from comparison of experimental (T1, T2) and calculated (WB T1_2) strains in axial and annular directions. The selected size of the elements is highlighted in the table.

5.2 Solution of the Models and Analysis of Results

After selecting the mesh size of finite elements, series of calculations were performed for each of the models I2, I3, I4. Internal pressure loading was carried out stepwise. Pressure was reset to zero after each step, bringing the pressure values on the plots with strain calculation results that were put here together with experimental data (Figs. 9, 10, 11, 12, 13, 14, 15, 16, 17 and 18).

Analytical results for undamaged and unrepaired zone for I2 model in elastic state (Figs. 19 and 20) have been found as follows [1]:

$$\sigma_{\text{axial}} = \frac{Pr}{2s} \tag{3}$$

$$\sigma_{\text{annular}} = \frac{Pr}{s} \tag{4}$$

$$\varepsilon = \sigma/E \tag{5}$$

where P is the internal pressure; r is the radius of the pipe; s is the pipe thickness; E is the Young's modulus.

General charts of analytical and WorckBench calculations for I2, I3, I4 models, annular strain are shown in Figs. 21 and 22.
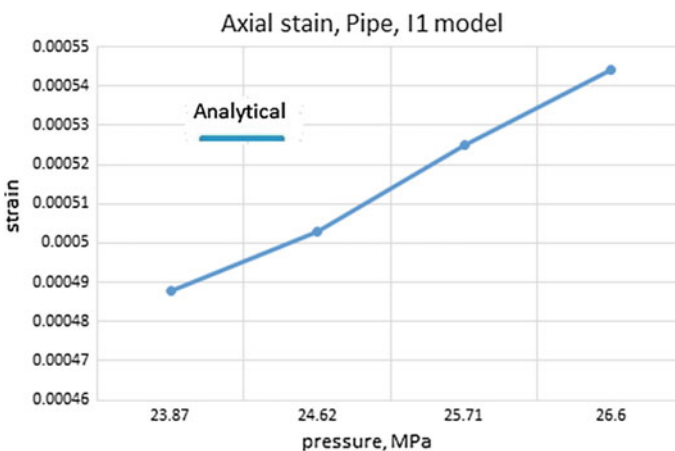
Fig. 9 Curves of axial strain and pressure (Pipe), I1 model
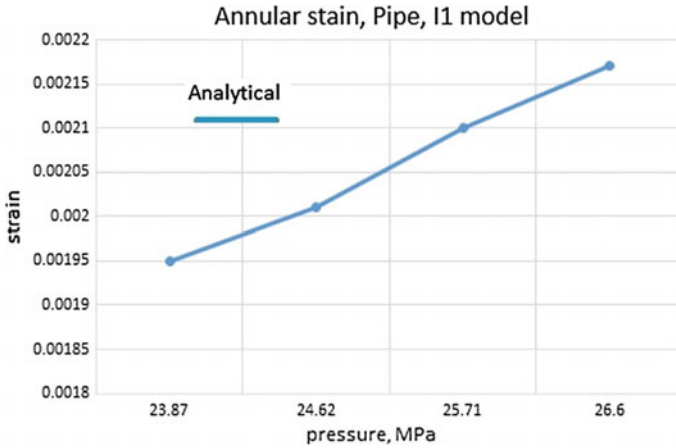
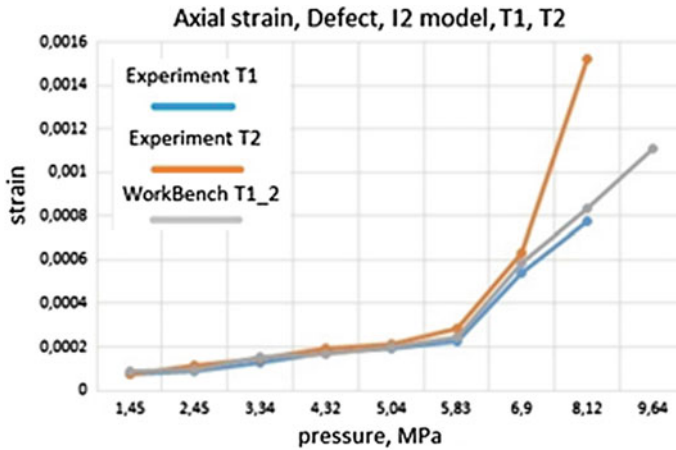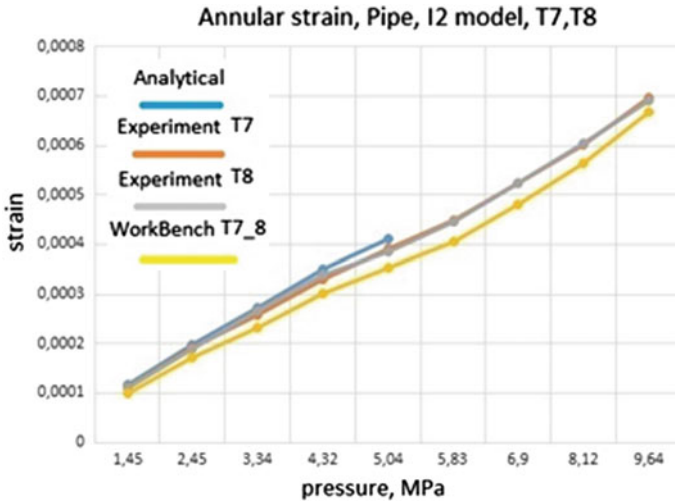**Fig. 10** Curves of annular strain and pressure (Pipe), I1 model

Fig. 11 Curves of axial strain and pressure (Defect), I2 model

Obtained results showed that the calculation models in the defect zone are close to the experimental data. The difference of the results for model I2 in the defect zone was from 3.87 to 9.84% in axial strain (Fig. 11) and from 5.81 to 12.79% in annular strain (Fig. 10). For the pipe far from the defect zone, the difference was from 3.53 to 7.52% in axial strain (Fig. 11) and from 4.16 to 11.4% in annular strain (Fig. 12).

The difference for model I3 in the defect zone was from 1.56 to 16.8% in axial strain (Fig. 13) and from 1.35 to 10.33% in annular strain (Fig. 14). For the pipe, the difference was from 0.73 to 6.27% in axial strain. On the wrap, difference was
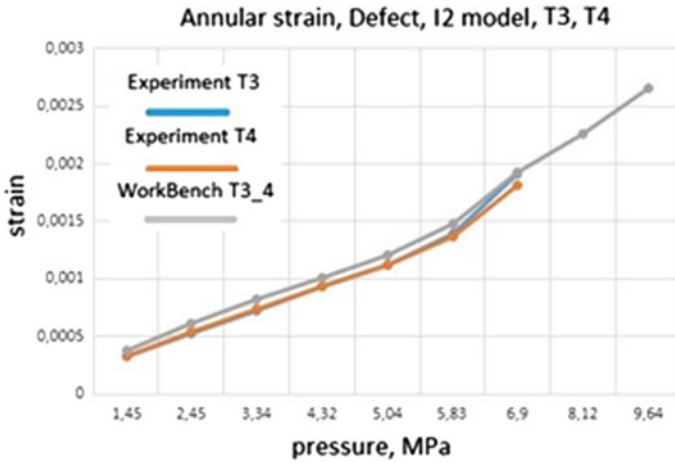
Fig. 12 Curves of annular strain and pressure (Defect), I2 model
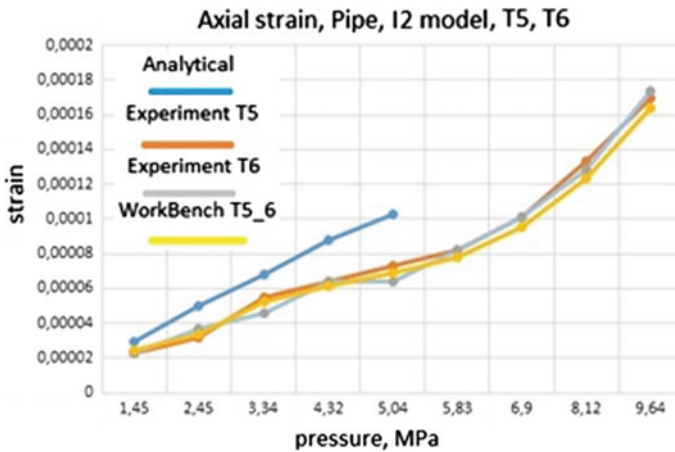
Fig. 13 Curves of axial strain and pressure (Pipe), I2 model

from 8.0 to 15.39% in axial strain (Fig. 15) and from 3.02 to 10.57% in annular strain (Fig. 16).

The difference for model I4 of the pipe was from 5.26 to 8.7% in axial strain (Fig. 17) and from 1.83 to 9.5% in annular strain (Fig. 18).

Probable reasons of difference between calculated and experimental strains are inaccuracy of data receiving from sensors in the experiments in some sections of the pipe and also the fact that a decision with the help of programs makes certain idealization calculations.

Fig. 14 Curves of annular strain and pressure (Pipe), I2 model
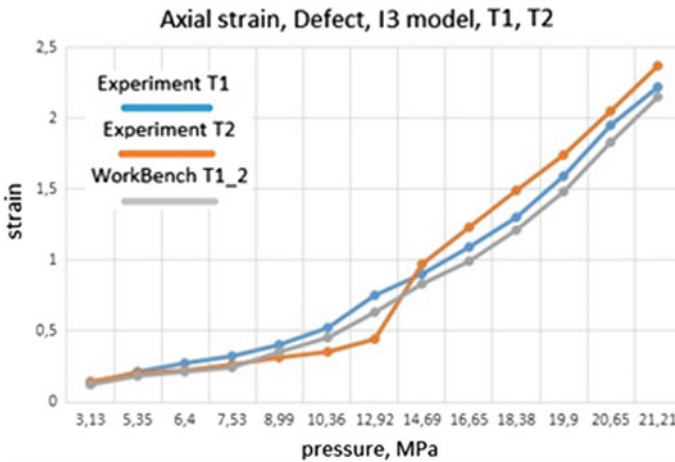
Fig. 15 Curves of axial strain and pressure (Defect), I3 model

Enough close agreement between experimental and calculated data can serve, on one hand, as confirmation of the authenticity of performed numerical calculations and, at the same time, as another indication of the efficiency of used composite repair system (Figs. 23 and 24).
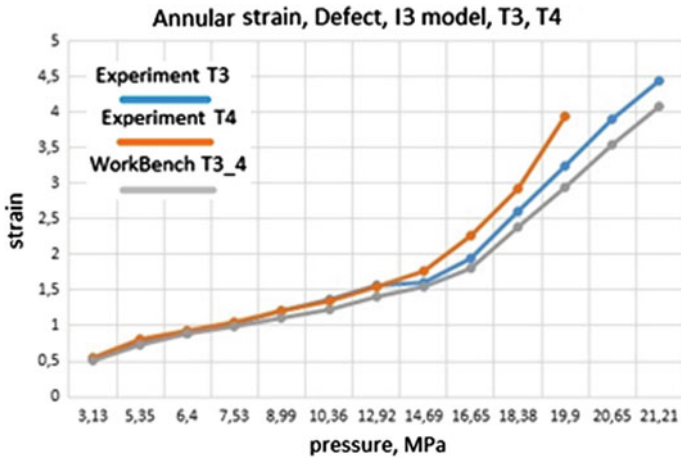
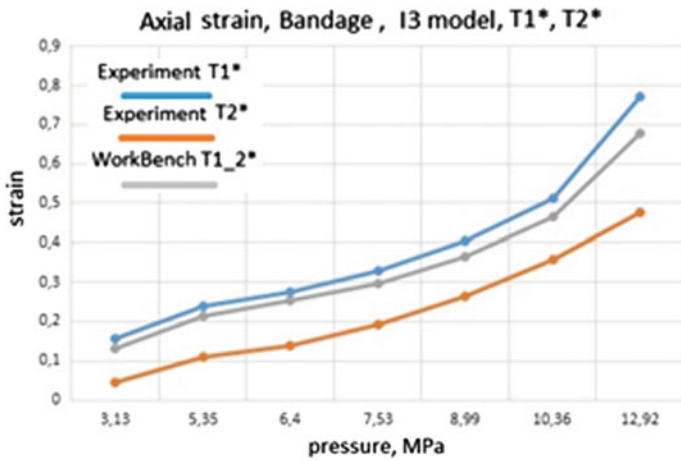**Fig. 16** Curves of annular strain and pressure (Defect), I3 model

Fig. 17 Curves of axial strain and pressure (Wrap), I3 model
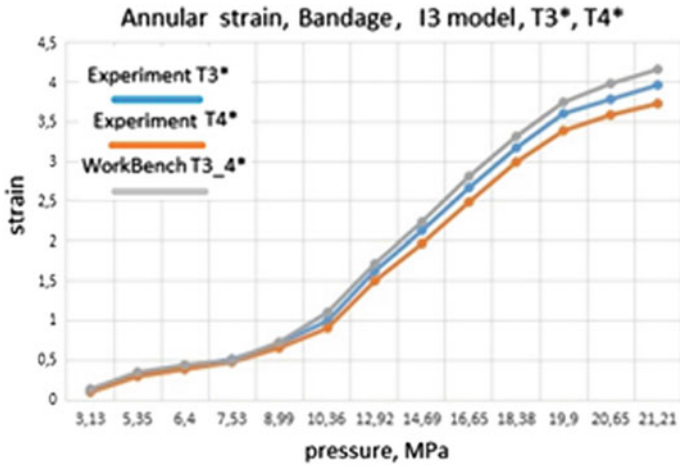
Fig. 18 Curves of annular strain and pressure (Wrap), I3 model
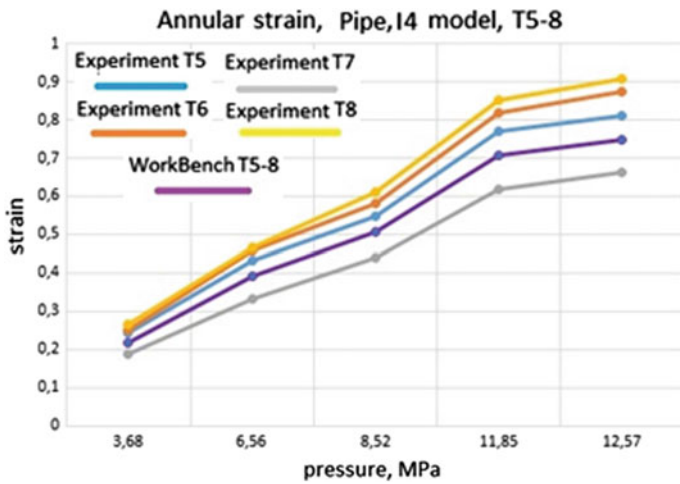

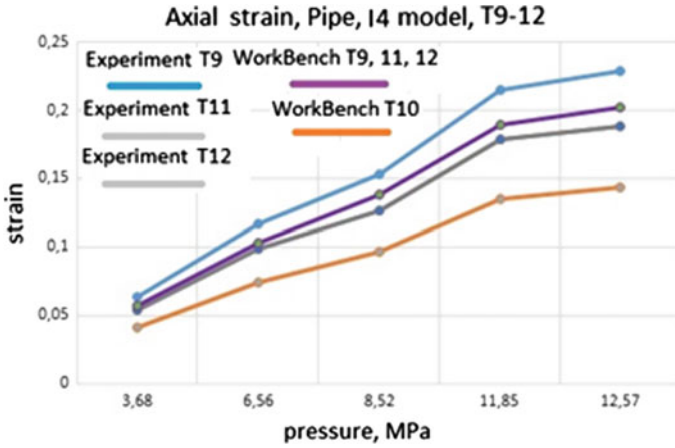**Fig. 19** Curves of annular strain and pressure (Pipe), I4 model

Fig. 20 Curves of axial strain and pressure (Pipe), I4 model
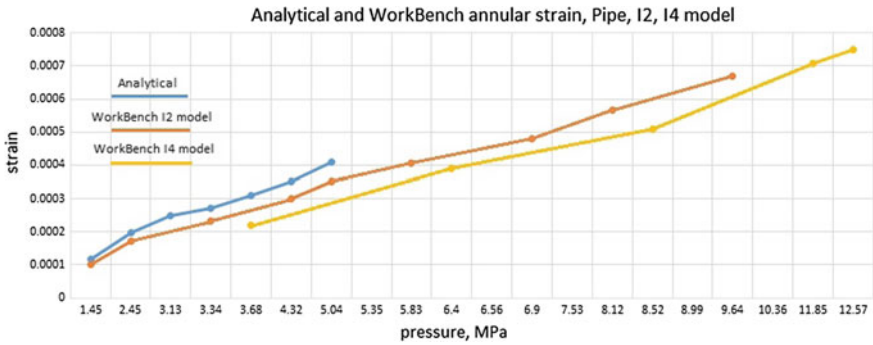

Fig. 21 General chart of analytical and Worck Bench calculations for I2, I4 models, annular strain
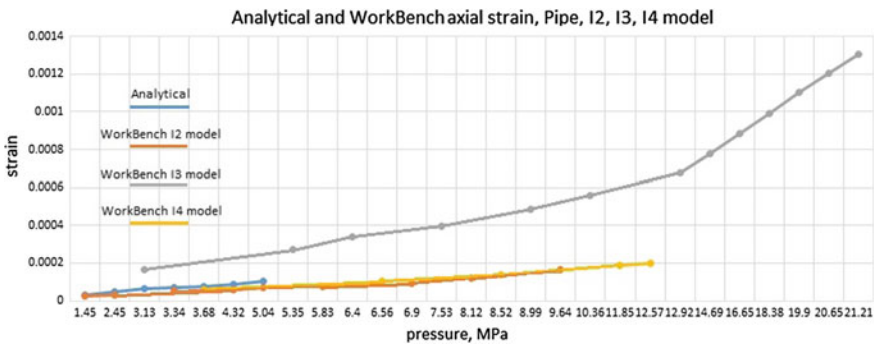

Fig. 22 General chart of analytical and Worck Bench calculations for I2, I3, I4 models, axial strain
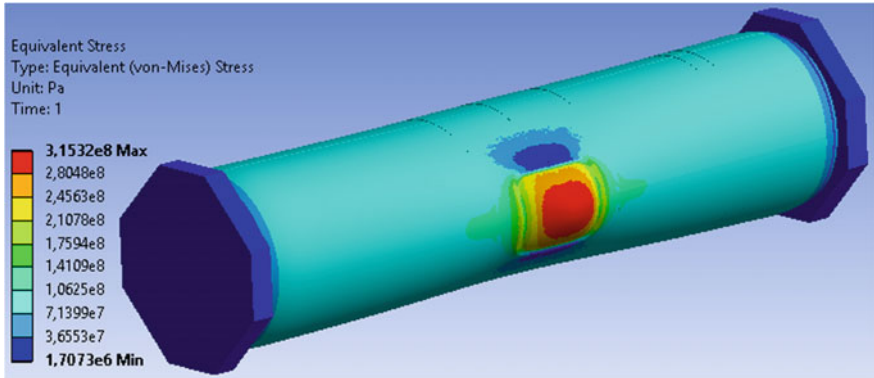
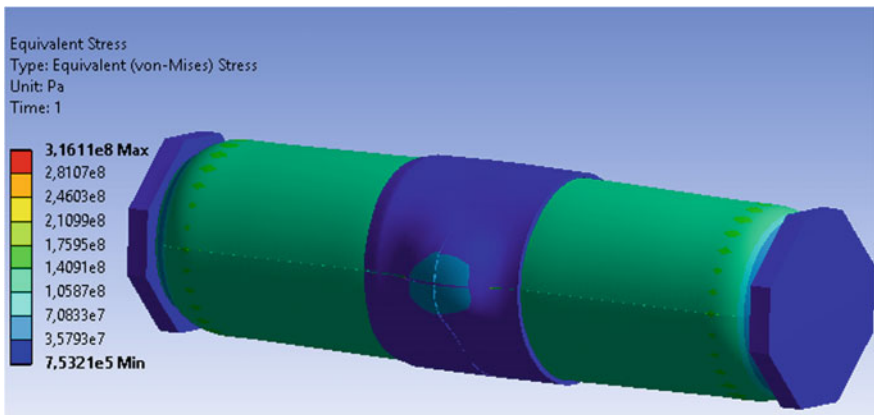**Fig. 23** Area of the defect zone of I2 and I3 models

Fig. 24 Curves of annular strain and pressure (models I1-I4)

6 Conclusions

Comparative analysis of changes in the volume, yield pressure, perimeter, deformations in the defect and loading diagrams of natural samples during their hydraulic tests as well as results of numerical modeling have demonstrated the efficiency of the used technology of the repair of a damaged pipeline section using composite material wraps.

References

1. V.M. Belayev, V.M. Mironov, *Design and calculation of elements of branch equipment. P.I: Thin wall vessels and apparatuses of chemical industry: Manual*. Tomsk, Tomsk Polytechnic University,(2003), 168 p